Binding of Calcium, Magnesium, and Target Peptides to Cdc31, the Centrin of Yeast Saccharomyces cerevisiae

ARTICLE *in* BIOCHEMISTRY · JUNE 2011

Impact Factor: 3.02 · DOI: 10.1021/bi200518d · Source: PubMed

5 AUTHORS, INCLUDING:

Simona Miron
Atomic Energy and Alternative Energies Com…
44 PUBLICATIONS **930** CITATIONS
SEE PROFILE

Dominique Durand
Université Paris-Sud 11
128 PUBLICATIONS **2,668** CITATIONS
SEE PROFILE

Claudia Chilom
University of Bucharest
14 PUBLICATIONS **85** CITATIONS
SEE PROFILE

Javier Perez
SOLEIL synchrotron
78 PUBLICATIONS **1,396** CITATIONS
SEE PROFILE

BIOCHEMISTRY
including biophysical chemistry & molecular biology

ARTICLE

pubs.acs.org/biochemistry

Binding of Calcium, Magnesium, and Target Peptides to Cdc31, the Centrin of Yeast *Saccharomyces cerevisiae*

Simona Miron,[*,⊥] Dominique Durand,[§] Claudia Chilom,[†,‡,#] Javier Pérez,[∥] and Constantin T. Craescu[†,‡,&]

[†]Institut Curie Centre de Recherche, Centre Universitaire Paris-Sud, 91405 Orsay Cedex, France
[‡]INSERM U759, Centre Universitaire Paris-Sud, 91405 Orsay Cedex, France
[§]Institut de Biochimie et Biophysique Moléculaire et Cellulaire, CNRS UMR 8619, Université Paris-Sud, 91405 Orsay, France
[∥]Synchrotron SOLEIL, BP 48, 91192 Gif-sur-Yvette Cedex, France

ABSTRACT: Cdc31, the *Saccharomyces cerevisiae* centrin, is an EF-hand calcium-binding protein essential for the cell division and mRNA nuclear export. We used biophysical techniques to investigate its calcium, magnesium, and protein target binding properties as well as their conformations in solution. We show here that Cdc31 displays one Ca^{2+}/Mg^{2+} mixed site in the N-terminal domain and two low-affinity Ca^{2+} sites in the C-terminal domain. The affinity of Cdc31 for different natural target peptides (from Kar1, Sfi1, Sac3) that we obtained by isothermal titration calorimetry shows weakly Ca^{2+}, but also Mg^{2+} dependence. The characteristics of target surface binding were shown to be similar; we highlight that the 1−4 hydrophobic amino acid motif, in a stable amphipathic α-helix, is critical for binding. Ca^{2+} and Mg^{2+} binding increase the α-helix content and stabilize the structure. Analysis of small-angle X-ray scattering experiments revealed that N- and C-terminal domains are not individualized in apo-Cdc31; in contrast, they are separated in the Mg^{2+} state, creating a groove in the middle of the molecule that is occupied by the target peptide in the liganded form. Consequently, Mg^{2+} seems to have consequences on Cdc31's function and could be important to stimulate interactions in resting cells.

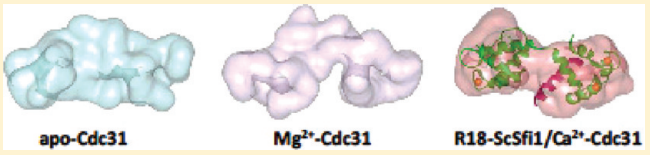

Centrins, members of the EF-hand superfamily, are acidic Ca^{2+} binding proteins closely related to calmodulin (CaM). They are highly concentrated in microtubule organizing centers (MTOC), which are called the centrosome in higher eukaryotes, spindle pool body (SPB) in yeast, and basal bodies in green algae.[1] The centrins play a critical role in the cellular duplication and segregation of the MTOC.[2] In the green algae *Chlamydomonas reinhardtii*, the flagellar excision is mediated by contractile fibers containing centrins, the contraction depending on the intracellular Ca^{2+} concentration.[3] Other cellular functions have been recently reported for centrins. In the nucleus, they are associated with the XPC/HR23B complex, initiating the nucleotide excision DNA repair mechanism.[4,5] In yeast, the centrins (Cdc31) are part of the Sac3−Thp1−Sus1 complex, being involved in the mRNA nuclear export;[6,7] Cdc31 specifically interacts with Sac3 protein. Centrins are also related to the proteasome and implicated in protein degradation.[8] How centrins could exert all these functions remain to be unveiled later.

The yeast SPB, a multilayer arrangement anchored into the nuclear envelope, attaches the half-bridge, a structure containing the centrin that has an essential role in the SPB duplication.[9−11] Temperature-sensitive mutants of Cdc31 affect the SPB duplication and arrest the cell cycle.[12] However, the molecular basis of centrin function in SPB or centrosomes is still unknown. Three protein targets of the Cdc31, localized in the half-bridge, were identified: Kar1,[13,14] Mps3,[15] and Sfi1.[16] *In vitro* and *in vivo* experiments provided evidence of the Cdc31 binding to the segment 237−255 of Kar1, a segment localized in an essential domain required for SPB duplication.[13,14] Whereas Kar1 is restricted to yeast, Sfi1 was identified in yeast SPB and human centrosomes. *Saccharomyces cerevisiae* Sfi1 (ScSfi1) and human Sfi1 (hSfi1) have 21 and 25 conserved repeats, respectively; each one is able to bind a molecule of centrin, in a 1:1 ratio. Thus, a single molecule of Sfi1 binds multiple molecules of centrins.[16−18]

The crystal structure of *Saccharomyces cerevisiae* centrins in complex with two or three repeats of ScSfi1 shows Sfi1 as a long α-helix with the centrins wrapped around.[17] The centrins are organized in two domains (N- and C-terminal), which are connected by a linker, and each is composed of two EF-hand motifs. The N-terminal Cdc31 domain is in a "closed" conformation (antiparallel EF-hand α-helices), whereas the C-terminal domain is in an "open" conformation (perpendicular EF-hand α-helices).[17] The central linker is bent in Cdc31, favorable to bring together the N-terminal Cdc31 and the N-terminal part of the Sfi1 repeat. Cdc31 binds Sfi1 via a deep hydrophobic cavity of the C-terminal domain, while its N-terminal has limited contacts with the N-terminal part of the Sfi1 repeat. The adjacent centrins have contacts: the C-terminal domain of one centrin interacts with the N-terminal domain of the next centrin, which is rotated by ∼65° along the Sfi1 helix as compared to the previous one. Electron microscopy of Sfi1 (containing 15 repeats)/centrin complexes has shown filaments whose length (59 nm) is not

Received: April 6, 2011
Revised: June 14, 2011

   dx.doi.org/10.1021/bi200518d | *Biochemistry* XXXX, XXX, 000–000

influenced by the calcium concentration.[17] Different models have been suggested for the structural organization of Sfi1/centrin complexes into the MTOC. Longitudinal interactions between centrins (along the Sfi1 helices)[17] or lateral interactions (perpendicular to the Sfi1 helices)[18] have been proposed. However, the cellular effect of these interactions and the role of calcium have not been demonstrated to date.

Other centrin targets (outside the MTOC) were identified, such as XPC (*Xeroderma pigmentosum* group C) and Rad4 proteins, in human and yeast cells, respectively. These proteins are involved in the nuclear excision repair (NER) mechanism. XPC interacts with human centrin 2 (HsCen2)[4] and hHR23 proteins. The yeast centrin is similarly present in the Rad4/ScRad23 repair complex,[8] and like in humans, Cdc31 interacts exclusively with the Rad4 protein.

The binding sites in the centrin targets are generally segments of ca. 20 amino acids, which adopt an amphipatipatic α-helix upon centrin binding, placing a hydrophobic triad (1−4−8 motif) on one face. A 17-residue fragment N^{847}−R^{863} of XPC (P17-XPC) shows a high affinity for HsCen2, and the centrin binding motif was identified as the hydrophobic triad $W^{848}{}_1L^{851}{}_4L^{855}{}_8$ (1−4−8 motif).[19,20] The centrin binding motifs in Sfi1 are also of 1−4−8 type (based on the position of the hydrophobic residues), but disposed in a reverse mode (8−4−1) as compared to the centrin binding motif in XPC, by a reverse orientation of the target α-helix. In the centrin binding motifs, the first and fourth positions are always occupied by hydrophobic residues, whereas the eighth position is less conserved (hydrophobic, but also charged or polar residues).

Centrins (∼20 kDa) are EF-hand calcium binding proteins and as other proteins from the CaM subfamily seem to act as a Ca^{2+} sensor. In their Ca^{2+}-loaded form their affinity for specific targets is higher than in the apo-form,[19,21] and this could modulate their cellular activity.[3] Currently, it is not clear if centrins are normally associated with their targets inside the cells or if their interactions are regulated by the intracellular Ca^{2+} concentration.

HsCen2, human centrin 3 (HsCen3), *Chlamydomonas reinhardtii* centrin (CrCen), and *Scherfellia dubia* centrin (SdCen), which are the best-characterized centrin family members, show very different Ca^{2+} binding properties. HsCen2 binds only one Ca^{2+} per molecule with a significant affinity (K_{dCa} = 30 μM), through the EF-hand IV;[22] Mg^{2+} does not influence Ca^{2+} binding. HsCen3 binds one Ca^{2+} with high affinity (K_{dCa} = 3 μM) and two Ca^{2+} with low affinity and binding to the high affinity site is strongly (K_{dMg} = 11 μM) antagonized by Mg^{2+}.[21] CrCen binds three Ca^{2+} per monomer; two with a high affinity (1−10 μM) in the N-terminal domain, and one with a moderate affinity, in the C-terminal domain, all the sites being Ca^{2+}-specific.[23] Like CrCen, SdCen exhibits three physiologically significant Ca^{2+}-binding sites: two in the N-terminal domain and one in the C-terminal domain.[24]

Cdc31 displays 63% sequence identity (75% similarity) with HsCen3 (the closest homologue of Cdc31) (Figure 1A) and likely shares many properties with the latter. It possesses four EF-hands, whereas EF1 and EF4 display canonical sequences close to those of CaM; EF2 at least should not bind Ca^{2+}. The capacity of EF3 motif to bind Ca^{2+} should be significantly decreased: its loop sequence exhibits an Asn instead of Glu in the −*Z* position, and in HsCen2 this substitution shows a 10 times lower binding affinity. The EF1 and EF4 have a Glu in the −*Z* position, which is favored as compared to an Asp residue in the EF hand functional motifs of EF hand proteins (Figure 1B). Mutations in EF1 and EF4 of Cdc31 resulted in a nonfunctional protein *in vivo*.[25]

Even though several studies of yeast centrin structure and biological functions have been performed, there are still unanswered questions. Three-dimensional structures of Cdc31 in complex with ScSfi1[17] or Sac3[26] fragments have been recently reported, but its calcium, magnesium, and protein target binding characteristics as well as the conformational exploration of different Cdc31 states were not investigated. By using different biophysical techniques, we focused on the structural, molecular, and thermodynamic basis of the cellular role of Cdc31, which belongs to the HsCen3 subfamily. We show here that Cdc31 has one high affinity Ca^{2+}/Mg^{2+} mixed site in the N-terminal domain and two lower affinity Ca^{2+} sites in the C-terminal domain. Ca^{2+} and Mg^{2+} binding induce conformational changes and a structural stabilization. Cdc31 interacts with high affinity (and a weakly dependence on Mg^{2+} and Ca^{2+} concentration) with different peptides from several natural targets (from Sfi1, Kar1, and Sac3). The 1−4 hydrophobic residues of the α-helical centrin binding motif of targets are critical for binding. Small-angle X-ray scattering (SAXS) experiments provided the low-resolution structure, in solution, of the apo-, Mg^{2+}-, and ScSfi1 peptide/Ca^{2+}-Cdc31 forms. As compared with the apo-form, the N- and C-terminal domains of Cdc31 are more individualized after Mg^{2+} binding, which could be helpful for target binding. Consequently, Mg^{2+} seems to have consequences on Cdc31's function and could stimulate *in vivo* interactions in resting cells.

MATERIALS AND METHODS

Biological Material. Cdc31 (18.7 kDa, 161 amino acids) was overexpressed and purified as previously described for HsCen2.[18,27] The protein was pure as analyzed by SDS-PAGE. In the present experiments we have used the wild-type protein and a substituted variant (C^{158} M) designed to avoid oxidation problems due to the Cys side chain. The peptides P19-ScKar1 (corresponding to the sequence K^{237}−K^{255} of the yeast Kar1 protein) and P18-ScSac3 (corresponding to the sequence K^{797}−I^{814} of the yeast Sac3 protein) were purchased from BIOFIDAL (Vaulx-en-Velin, France) and Hybio (Shenzhen Hybio Engineering Co., Shenzhen, China). The peptides R18-ScSfi1, R19-ScSfi1 (corresponding to the I^{680}−R^{699} and E^{710}−K^{729} sequences of the yeast Sfi1 protein), R17-hSfi1 (sequences R^{641}−T^{660} and S^{649}−T^{660} of the human Sfi1), and P11-XPC (sequence R^{843}−K^{853} of the human XPC protein) were purchased from GeneCust (Dudelange, Luxembourg). All the peptides were acetylated at the N-terminal end and amidated at the C-terminal end. Purity was greater than 95%, as assessed by high-pressure liquid chromatography analysis.

Metal Removal and Cation Binding. Cdc31 was precipitated with 3% trichloroacetic acid and passed through a 40 × 1 cm Sephadex G-25 column, equilibrated in 50 mM Tris-HCl, pH 7.5, 150 mM KCl (buffer A). Typically, the contamination represents less than 2% of the total binding capacity. Ca^{2+} and Mg^{2+} concentrations were determined with a Perkin-Elmer 2380 atomic absorption spectrophotometer. Flow dialysis on 40 μM Cdc31 was carried out in the absence or in the presence of Mg^{2+} at 25 °C, in buffer A according to the modified method of Colowick and Womack.[28] The analysis of the raw data and the evaluation of the binding parameters were done as previously

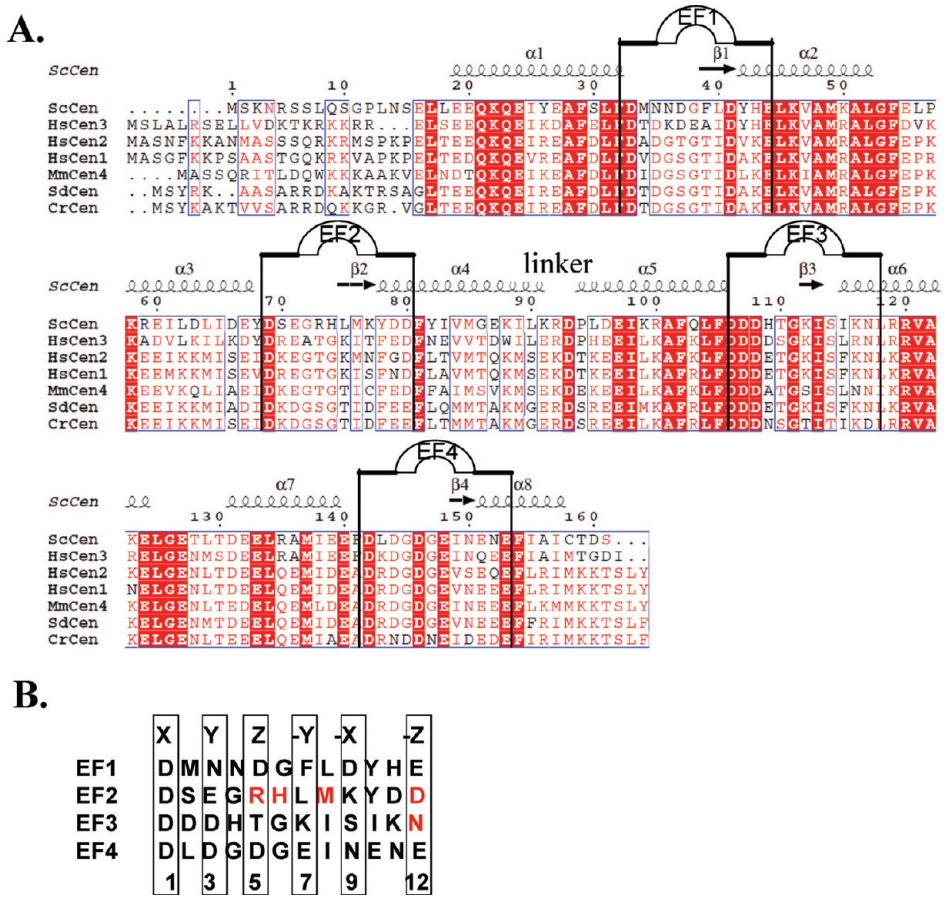

Figure 1. (A) The sequence alignment between different centrins was performed with MULTALIN.[48] The sequence of *Saccharomyces cerevisiae* centrin (ScCen) was aligned to the human centrins (HsCen1, HsCen2, HsCen3), *Scherfellia dubia* centrin (SdCen), *Chlamydomonas reinhardtii* centrin (CrCen), and *Mus musculus* centrin 4 (MmCen4). The secondary structures derived from the crystal structure of Cdc31 in complex with the Sfi1 fragment (2GV5.pdb) are indicated on the top of the sequences. ESPript[49] was used for the graphical representation. The identical residues over all sequences are shown on a red background, and conservative residues are colored in red. The four EF-hand loop motifs are indicated. (B) The ion binding EF-hand loop motifs in Cdc31.

described.[29] The data were analyzed with the Adair equation for three binding sites (see ref 21). The antagonism between Ca^{2+} and Mg^{2+} was tested with the competition equation for each site, $K'_{Ca}/K'_{Ca.app} = 1 + K'_{Mg.comp}(Mg^{2+})$, where K'_{Ca} and $K'_{Ca.app}$ are the intrinsic Ca^{2+} binding constants for a given site in the absence and the presence of Mg^{2+}, respectively, and $K'_{Mg.comp}$ is the calculated Mg^{2+} binding constant for this site.

Direct Mg^{2+} binding was studied by equilibrium gel filtration at room temperature as reviewed previously,[29] in buffer A containing 50 μM EGTA to complex contaminating Ca^{2+}.

Fluorescence Spectroscopy. Tyr fluorescence spectra and isotherms were measured at 20 °C using a Perkin-Elmer LS 50B spectrofluorimeter. The protein concentration was 12 μM. Trp fluorescence measurements were performed at 20 °C, using a Jasco FP777 spectrofluorimeter. The wavelength for excitation was 295 nm, and the fluorescence emission was monitored with a band-pass of 5 nm between 305 and 400 nm. The solution of free peptide gives a maximum of fluorescence emission at 350 nm. The fluorescence emission of Trp of P18-ScSac3 was followed as a function of the Cdc31 concentration. The binding of Cdc31 to the peptide (2 μM) affects the fluorescence of the peptide, and the maximum of fluorescence emission is blue-shifted (to 330 nm). The fluorescence intensity at 330 nm as a function of protein concentration was fitted to a one-site binding model using Origin 7.0 software (OriginLab Corp.). The buffer contained 50 mM Mops, pH 7.2, 100 mM NaCl, 2 mM $CaCl_2$.

Interaction with Hydrophobic Probes. The hydrophobic exposure of Cdc31 was followed by monitoring the fluorescence of TNS as previously described.[21] The fluorescence enhancement of TNS by Cdc31 is about 5 times weaker than that of other centrins. Therefore, the protein concentrations of 10 μM were used in these experiments.

Circular Dichroism (CD). CD experiments have been performed on a Jasco J-715 spectropolarimeter equipped with a Peltier temperature control unit. Far-UV CD spectra were recorded between 195 and 260 nm, at 20 °C, using 1 mm quartz cells. The spectra were acquired as an average of five scans, with a scan speed of 50 nm/min and a response time of 2 s. The spectrum of the buffer was subtracted from the sample spectra. The Cdc31 samples were at 13.5 μM in 10 mM Tris buffer, pH 7.0, 100 mM NaCl. The apo-form was obtained by the addition of 2 mM EDTA. The Mg^{2+}-Cdc31 and Ca^{2+}-Cdc31 forms contained 2 mM EGTA and 2 mM $MgCl_2$ or 2 mM $CaCl_2$, respectively. Temperature denaturation (between 5 and 95 °C) was followed recording the ellipticity at 222 nm, with a temperature increase rate of 1 °C/min. The thermal unfolding process was almost reversible (~95% of the CD signal was recovered after thermal denaturation). Thermal denaturation profiles in

dx.doi.org/10.1021/bi200518d |*Biochemistry* XXXX, XXX, 000–000

Figure 4B were analyzed by a nonlinear least-squares fit assuming a two-state model according to the equation

$$y(T) = y_n + s_n T + \frac{exp[-(\Delta H_m/R)(1/T - 1/T_m)](A + (s_d - s_n)T)}{1 + exp[-(\Delta H_m/R)(1/T - 1/T_m)]} \quad (1)$$

where y_n is the y intercept, s_n is the initial slope, s_d is the slope at the end of the denaturation, A is the amplitude of the denaturation transition, T_m is the midpoint of the thermal denaturation, and R is the universal gas constant (kcal mol^{-1}).

The far-UV CD spectra have been analyzed for the secondary structure content by CDPRO software package.[30] Different tools have been developed to analyze the CD spectra and use different secondary structure calculation algorithms. The CDSSTR analysis procedures were used to calculate the secondary structures of the Cdc31 protein.

Isothermal Titration Calorimetry (ITC). ITC titrations were performed on a VP-ITC calorimeter (GE, Healthcare). Prior to the measurements all the solutions were degassed under vacuum for the elimination of bubbles. The ITC measurements were done at 30 °C, and solutions were prepared in the same buffer containing 50 mM Mops buffer, pH 7.4, 100 mM NaCl. For the interaction between the protein and the peptides the buffer solution contained 2 mM $CaCl_2$ or 2 mM EDTA or 2 mM EGTA and 2 mM $MgCl_2$. Cdc31 at 10−25 μM (in the calorimeter cell) was titrated with the peptides (100−200 μM). The automatic injections of 5−10 μL with 240 or 280 s intervals between each injection have been used. The first injection (2 μL) was ignored in the final data analysis. To correct for the heat effects of dilution, control experiments were performed at the same concentrations. Thermodynamic parameters, ΔH (enthalpy change), n (stoichiometry), and K_a (equilibrium binding constant) were obtained by nonlinear least-squares fitting of the experimental data using the Origin software provided with the instrument. The free energy of binding (ΔG) and entropy (ΔS) were obtained using the classical thermodynamic formulas $\Delta G = -RT \ln K_a$ and $\Delta G = \Delta H - T\Delta S$, where R is the gas constant and T is the absolute temperature in kelvin.

Small-Angle X-ray Scattering (SAXS) Experiments. SAXS experiments were carried out on the SWING beamline at the SOLEIL synchrotron radiation facility in France. The incident beam energy was 12 keV, and the sample to detector (Aviex CCD) was set to 1820 mm. The scattering vector range was $0.01 < q < 0.5$ Å^{-1}. A concentrated sample (6−22 mg/mL) was injected into a size-exclusion column (SHODEX KW402.5) using an Agilent high performance liquid chromatography system and eluted directly into the SAXS flow-through capillary cell at a flow rate of 150 μL min^{-1}. Following the procedure described by David and Pérez,[31] SAXS data were collected online throughout the whole elution time, with frame duration of 2 s and a dead time between frames of 0.5 s. For each frame, the protein concentration (about 1 or 2 mg/mL at the top of elution peak) was estimated from UV absorption at 280 nm using a spectrometer located immediately upstream of the SAXS cell. Selected identical frames corresponding to the main elution peak were averaged. A large number of frames were collected during the first minutes of the elution flow and averaged to account for buffer scattering, which was subsequently subtracted from the averaged protein signal. The scattered intensities were displayed on an absolute scale using the scattering by water. Data analysis and *ab initio* shape calculations were performed using the programs of Svergun's team (PRIMUS, GNOM, GASBOR, CRYSOL, DAMAVER, and CORAL).[32] SAXS experiments were performed on the apo-Cdc31 (10 mM EDTA), the Mg^{2+}-Cdc31 form (10 mM EGTA, 10 mM $MgCl_2$), and the complex R18-ScSfi1/Cdc31 (1:1 ratio and 10 mM $CaCl_2$). The buffer was 50 mM Mops, 200 mM NaCl, pH 7.1.

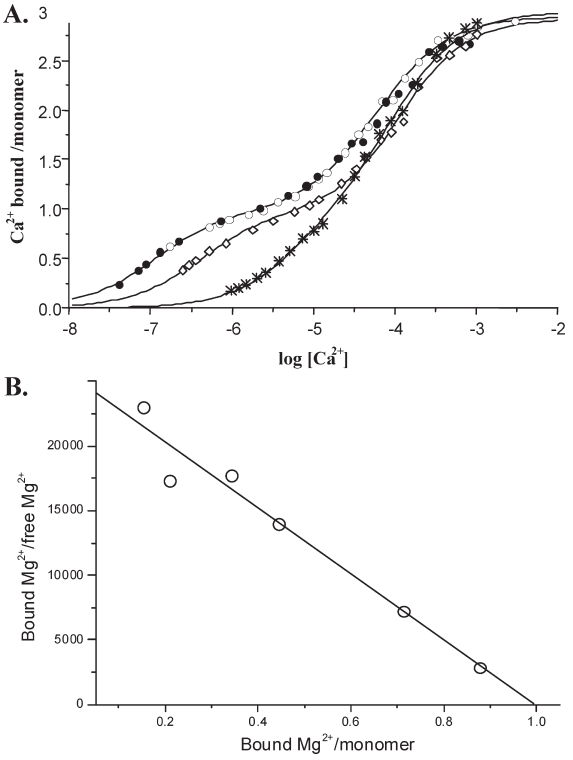

Figure 2. Binding of Ca^{2+} and Mg^{2+} to Cdc31. (A) Direct Ca^{2+} binding to recombinant Cdc31 was monitored by flow dialysis at 25 °C in 50 mM Tris/HCl (pH 7.5) and 150 mM KCl (buffer A). The protein concentration is 25 μM. Binding in the absence (filled and empty cercles, duplicated experiment) or presence of 0.2 (squares) and 5 mM Mg^{2+} (stars). The solid lines are the theoretical isotherms calculated with the Adair equation for three sites with the intrinsic constants listed in Table 1. (B) The Scatchard plot of the direct binding of Mg^{2+} to Cdc31 monitored by equilibrium gel filtration in buffer A containing 30 μM EGTA.

RESULTS

Divalent Cation Binding Studies. Flow dialysis on apo-Cdc31 in the absence of Mg^{2+} yielded a biphasic isotherm (Figure 2A) with one site of very high affinity (K_{dCa} of 0.3 μM) and two sites of much lower affinity (K_{dCa} of 28 and 41 μM). Table 1 shows the intrinsic association constants K'_n extracted from the analysis of the ensemble of the binding data. The Mg^{2+} effect on Ca^{2+} binding is clearly highlighted for the high affinity site: at 5 mM Mg^{2+} the apparent K_{dCa} for the high-affinity site is 16 μM. Using the competition equation (see Materials and Methods), one observes that Mg^{2+} directly competes with Ca^{2+}: the K_{Mgcomp} is around 90 μM. As in the case of HsCen3,[21] the high affinity site is of the Ca^{2+}/Mg^{2+} mixed type. The low affinity sites are much less affected by increasing Mg^{2+} concentrations until 5 mM. Using the competition equation, we

Table 1. Intrinsic Ca^{2+} Binding Constants of Cdc31 at Different Mg^{2+} Concentrations Derived from the Stoichiometric Constants Which Were Obtained by Fitting All the Data to the Adair Equation for Three Sites

(Mg^{2+}) (mM)	K'_1 (M^{-1})	K'_2 (M^{-1})	K'_3 (M^{-1})
0	3.0×10^6	3.5×10^4	2.4×10^4
0.2	8.2×10^5	1.5×10^4	1.5×10^4
5	6.3×10^4	1.7×10^4	1.4×10^4

obtained for the low affinity sites a K_{dMg} of around 3−4 mM, i.e., values also obtained in the case of CaM.[33]

Direct Mg^{2+} binding was studied with equilibrium gel filtration (in buffer A containing 50 μM EGTA). An isotherm without any cooperativity has been obtained, with a K_{dMg} value of 44 μM (very similar to the value obtained using competition equation) and a stoichiometry of 0.99 (Figure 2B). Sites of low affinity for Mg^{2+} (K_d > 500 μM) cannot be detected by equilibrium gel filtration.

Intrinsic fluorescent groups are often good markers of the conformational states of a protein. Cdc31 possesses five Tyr residues, all located in the N-terminal domain (Tyr 42 and Tyr 78 being in the EF1 and EF2 sites, respectively) (Figure 1A). Consequently, Tyr fluorescence experiments give information about the affinity and selectivity of sites located in the N-terminal domain. The Tyr residues are conformation-sensitive since upon denaturation with 4 M guanidine-HCl the fluorescence decreases 1.4-fold concomitant with a 3 nm blue shift of the maximal fluorescence intensity. Upon binding of Ca^{2+} or Mg^{2+} (1 mM) there is a 1.2-fold fluorescence increase and the spectra of the Mg^{2+}- and Ca^{2+}-loaded forms are indistinguishable (Figure 3A). The simultaneous addition of the two cations does not increase the effect, indicating that Ca^{2+} and Mg^{2+} compete with each other.

The Mg^{2+} titration curve in the presence of 50 μM EGTA to neutralize contaminating Ca^{2+} is shown in Figure 3B. Although the measurements were performed until a $[Mg^{2+}]$ concentration (2.5 mM) lower than the K_d value of the low affinity sites (3−4 mM), it clearly appears that the curve can be described by a transition with a $[Mg^{2+}]_{0.5}$ of 66 μM close to the K_d value of the Ca^{2+}/Mg^{2+} high affinity mixed site. We can conclude that the Ca^{2+}/Mg^{2+} high affinity mixed site is located in the N-terminal domain.

Conformation Effects of Ca^2, Mg^{2+}, and Peptide Binding on Cdc31. Far-UV CD spectroscopy has been used to follow the secondary structure changes in Cdc31 after Mg^{2+}, Ca^{2+}, or peptide R18-ScSfi1 binding (in the presence of $CaCl_2$). The apo-Cdc31 has a CD spectrum with a positive 196 band and two negative 208 and 222 nm bands, which are characteristics for a rich α-helix conformation (Figure 4A). The ion binding (Mg^{2+} or Ca^{2+}) induces similar CD spectral changes (the 196, 208, and 222 nm bands have comparable increases): the stable α-helical secondary structure of the protein increases from 38.5% α-helices (in apo-Cdc31 state) to 44.6% and 44.5% α-helices in the presence of Mg^{2+} and Ca^{2+}, respectively. A small additional increase of the α-helix content is observed when R18-ScSfi1 peptide is added at 1:1 ratio, in the Ca^{2+} saturated form. The peptide alone, at the same concentration, has a CD spectrum with negative peaks, at 199 and 222 nm, indicating a low proportion of α-helix in equilibrium with a high proportion of random coil (Figure 4A). The α-helical content for R18-ScSfi1/Cdc31 complex (estimated by CDPRO software) is of 47.5%, in agreement with the α-helical secondary structure observed in the

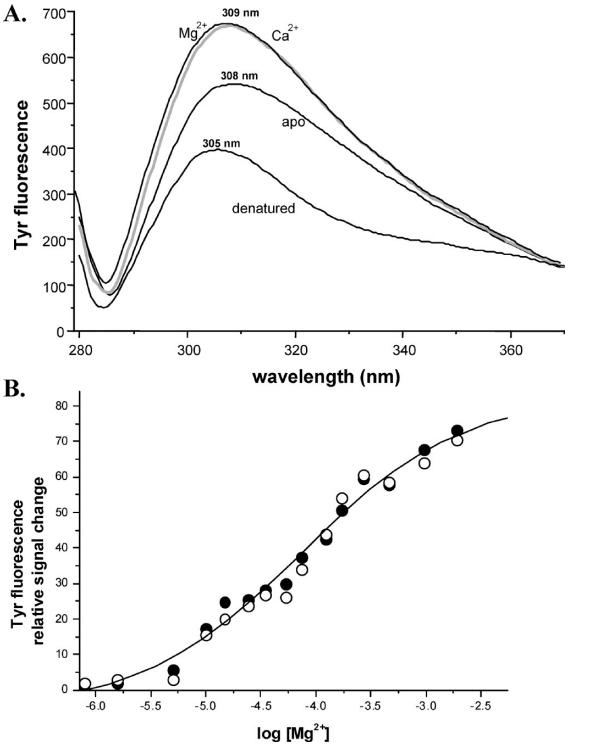

Figure 3. (A) Ca^{2+}- and Mg^{2+}-dependent conformational changes monitored by Tyr fluorescence at 25 °C, after excitation at 278 nm. 12 μM Cdc31 in buffer A *plus* 50 μM EGTA (apo), 1 mM Mg^{2+} *plus* 50 μM EGTA (gray), or 1 mM Ca^{2+}. The denatured conformation was measured after addition of 4 M guanidine-HCl. All spectra were normalized to the same protein concentration. (B) Mg^{2+} titration (duplicated experiment) of the fluorescence change in the presence of 50 μM EGTA. The line is calculated with the Adair equation for one site per monomer and yields a K_D of 66 μM.

crystal structure of Cdc31/Sfi1 complexes.[17] In these structures, the Sfi1 peptide is completely folded into a α-helix.[17] The small increased α-helical content, in solution, for the complex, as compared to the Ca^{2+} or Mg^{2+} forms, must be mostly due to the partial α-helix folding of the peptide. The same behavior was also observed in the NMR solution structure of C-HsCen2/R17-hSfi1-20 complex, in which 10 from the 20 residues of R17-hSfi1-20 peptide are organized into a α-helix.

CD thermal denaturation (between 5 and 95 °C) was performed to find out if the ions or the ligands (i.e., the peptide) induced thermal stabilization in Cdc31 (Figure 4B). In order to compare the thermal stability of different Cdc31 states, the CD thermal denaturation curves were fit with eq 1 (see Materials and Methods), assuming a two-state unfolding transition. We are aware that this model has limitiations. Cdc31 is a muldidomain protein with a complex unfolding process (structural stability and unfolding are probably different in each of both EF-hand domains). Moreover, for the Mg state, the experiments were performed at 2 mM $MgCl_2$, in the range of the K_d of the low affinity sites (e.g., 3−4 mM at the experimental conditions of flow dialysis). Therefore, we cannot exclude the presence of several populations (the low-affinity sites being probably not completely saturated, at the experimental conditions of CD). However this two-state model is sufficient to prove that Mg^{2+} and Ca^{2+} binding lead to a structural stabilization of the protein. The apo-form displays a CD melting curve with a cooperative

dx.doi.org/10.1021/bi200518d |*Biochemistry* XXXX, XXX, 000–000

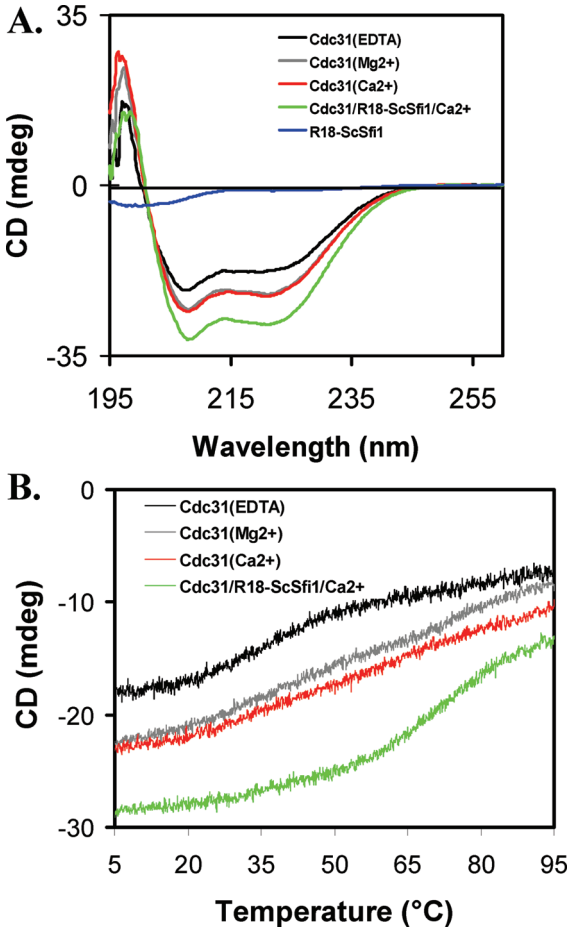

Figure 4. CD spectra of Cdc31. (A) Far-UV CD spectra at 20 °C of 13.5 μM Cdc31 in 10 mM Tris/HCl, pH 7.0, 100 mM NaCl, in the presence of 2 mM EDTA, (the apo-form, black), Mg^{2+}-Cdc31 (2 mM $MgCl_2$ and 2 mM EGTA, gray), Ca^{2+}-Cdc31 (2 mM $CaCl_2$, red), and Cdc31/R18-ScSfi1 (1/1 ratio, in the presence of 2 mM $CaCl_2$, green). The CD spectrum of R18-ScSfi1 peptide (13.5 μM) is colored in blue. (B) Thermal denaturation curves recorded between 5 and 95 °C at 222 nm, for the apo-Cdc31, Mg^{2+}-Cdc31, Ca^{2+}-Cdc31, and R18-ScSfi1/Cdc31 (1:1) complex. The samples are represented by the same colors like in panel A.

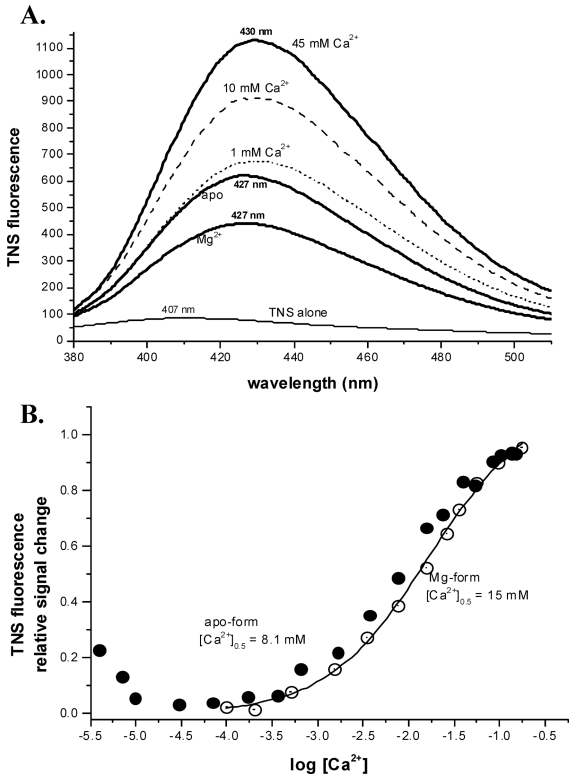

Figure 5. Ca^{2+}-dependent exposure of hydrophobic side chains. Hydrophobic exposure was measured at 25 °C in buffer A with the hydrophobic probe TNS. (A) Emission fluorescence spectra of TNS alone (at concentration of 100 μM) and with 8 μM Cdc31 in the presence of 100 μM EGTA (apo), 1 mM Mg^{2+} *plus* 100 μM EGTA (Mg^{2+}) or 1 mM (dotted), 10 mM (dashed) or 45 mM Ca^{2+} (Ca^{2+}). (B) Ca^{2+} titration in the absence (solid circles) and presence (open cirles) of 1 mM Mg^{2+}.

thermal transition, with a midpoint temperature of 36.7 °C. The Ca^{2+}- and Mg^{2+}-Cdc31 forms shows almost the same thermal denaturation curves, indicating that Ca^{2+} and Mg^{2+} binding to Cdc31 have almost similar effect on the conformation of Cdc31. Like HsCen3, but different from HsCen2, the Mg^{2+}- and Ca^{2+}-Cdc31 shows a regularly decrease of ellipticity (a large transition) from 20 to 95 °C, with the midpoint of the transition of 65 and 58 °C, respectively. The ions induce structural stabilization in Cdc31, which has been also observed for others members of this family of proteins.[19,21,24] The R18-ScSfi1/Cdc31 complex shows a cooperative unfolding and an increase in the midtemperature transition (72.4 °C), indicating a strong stabilization of Cdc31 by the R18-ScSfi1 peptide.

A specific conformational probe for CaBPs is the fluorescence of the hydrophobic TNS, whose signal is enhanced after exposure of hydrophobic surfaces.[34] Figure 5A shows that the apo-form enhances the TNS fluorescence 7-fold and shifts the maximum from 407 to 427 nm, therefore indicating a large exposure of hydrophobic area. Addition of 1 mM Mg^{2+} leads to a 1.4-fold fluorescence decrease as compared to the apo-state. Interestingly, the addition of Ca^{2+} to the apo-form shows a biphasic response of TNS fluorescence enhancement (Figure 5B). At Ca^{2+} concentrations between 10 and 300 μM a weak fluorescence decrease is observed as compared to the apo-state. This conformation persists up to 300 μM Ca^{2+}, i.e., largely above the concentrations that saturate the two low affinity sites. Much higher Ca^{2+} concentrations lead to a fluorescence enhancement of 2.5-fold. The Ca^{2+} titration of this step yielded $(Ca^{2+})_{0.5}$ values (Figure 5B) considerably above the physiological Ca^{2+} concentration inside a yeast cell,[35] and its physiological relevance is therefore not clear. High concentrations of Mg^{2+} do not lead to any fluorescence increase.

Analysis of SAXS experiments provided complementary information on the conformation of Cdc31, in the apo- and holo-states (Mg^{2+}-Cdc31 and R18-ScSfi1/Ca^{2+}-Cdc31). Complexes of Cdc31 with Ca^{2+} could not be studied because they polymerize too strongly at the concentration used for SAXS experiments. Interestingly, this behavior is not observed despite some oligomerization also occurs for Mg^{2+}-Cdc31. By using the size-exclusion chromatography setup installed on the SWING beamline (SOLEIL facility), it was possible to study the three species by SAXS in monomeric form free from oligomers.

Dimensions of the protein (radii of gyration R_g and maximum distances D_{max}) were extracted from the analysis of the scattering curves $I(q)$ by using the well-known Guinier approximation ln

Table 2. Radius of Gyration R_g and the Maximum Distances D_{max} Values Deduced from the Experimental Curves for the Studied Samples and from the Calculated Curves Based on Crystal Structures

	R_g (Å)	D_{max} (Å)
Cdc31 (EDTA)	22.7 ± 0.5	81 ± 5
Cdc31 (Mg^{2+})	23.6 ± 0.5	78 ± 5
Cdc31 (R18-ScSfi1/Cdc31/Ca^{2+})	22.1 ± 0.5	72 ± 5
Crystal 2GV5B (without peptide)	20.9	64
Crystal 2GV5B (with peptide)	20.1	64

$I(q) = \ln I(0) - q^2R_g^2/3$ in the $qR_g < 1$ range and from the pair distance distribution function $P(r)$, deduced from $I(q)$ using the program GNOM.[36] $P(r)$ represents the average number of neighboring atoms from any pair atom at a distance r. R_g and D_{max} values are given in Table 2, together with the values determined from the crystal structure of R18-ScSfi1/Cdc31 complex (2GV5, molecule B), and the values obtained from the same PDB file from which the peptide was removed. Despite the 2GV5 structure was obtained in the absence of Ca^{2+}, the conformation of Cdc31 in the complex is nearly the same in the presence and in the absence of Ca^{2+}.[17]

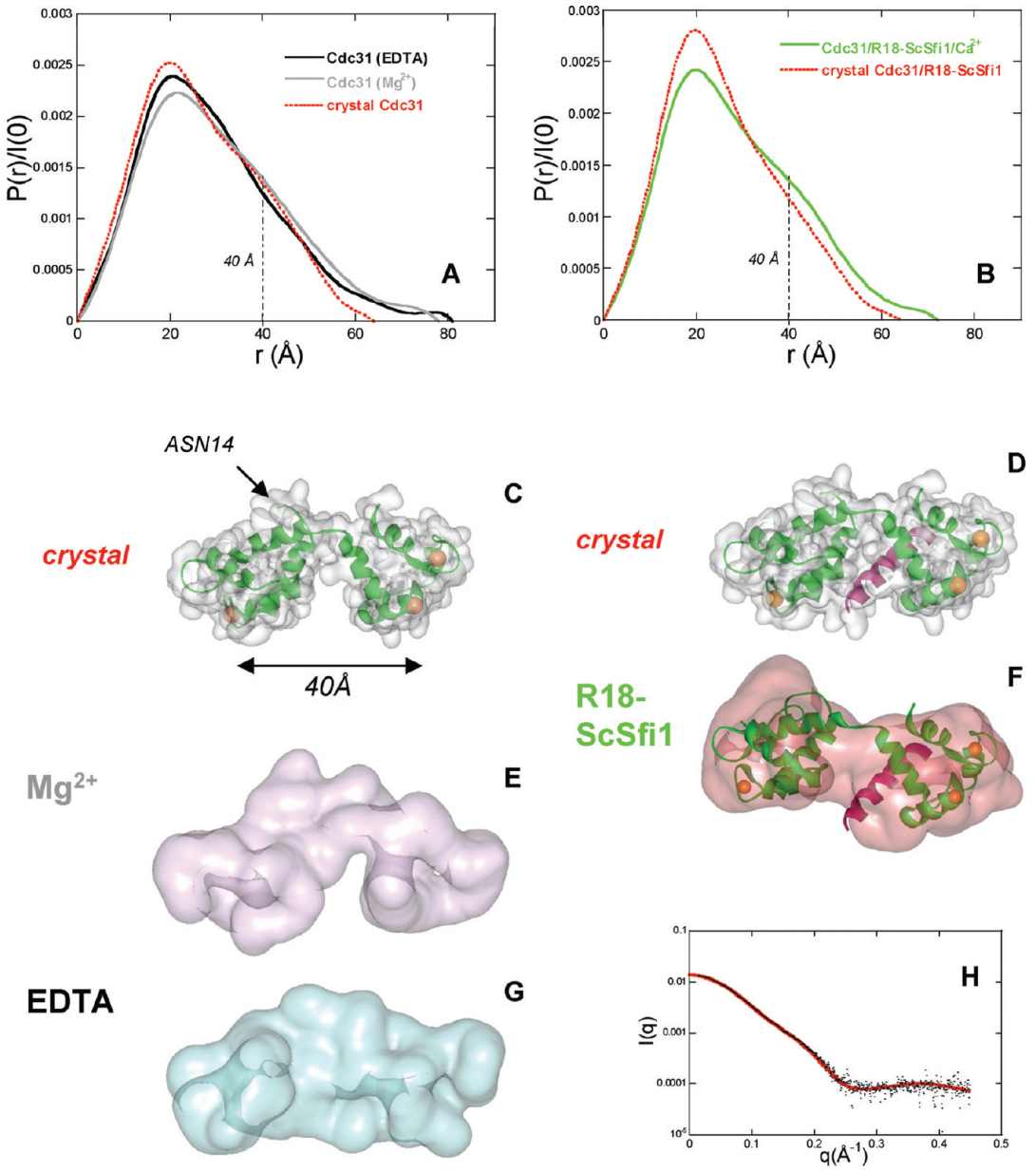

Figure 6. (A) Distance distribution function $P(r)$ of apo-Cdc31 (black), Mg^{2+}-Cdc31 (gray), and from crystal structure 2GV5 (molecule B) without peptide (red). (B) Distance distribution function of R18-ScSfi1/Cdc31 complex (green) and from crystal structure 2GV5 (molecule B) with peptide (red). (C) Crystal structure 2GV5 (molecule B) without peptide. The three Ca^{2+} sites are shown as orange spheres. The envelope of the protein is shown in gray. (D) Crystal structure 2GV5 (molecule B) with peptide (pink). (E) Most typical envelope deduced from the scattering curve $I(q)$ using the program GASBOR for Mg^{2+}-Cdc31 (F) Most typical envelope obtained for the complex R18-ScSfi1/Cdc31. The conformation obtained using the program CORAL, which moved the N-terminal domain, is superimposed. (G) Most typical envelope for the apo-Cdc31. (H) R18-ScSfi1/Cdc31: comparison of the experimental curve (black dots) with the calculated one (red line) from the conformation shown in (F).

The presence of Mg^{2+} as well as the addition of the peptide R18-ScSfi1 has only a moderate effect on the dimensions of the protein (which are slightly higher than those corresponding to the crystal structure, probably due to the flexible 13 residues N-terminal part). The N-terminal end (M^1-L^{13}) of Cdc31 is not visible in the crystal structure,[17] but this fragment accounts for 7 and 8% of the full length of R18-ScSfi1/Cdc31 and apo-Cdc31, respectively. However, a closer examination of the distance distribution function $P(r)$ and of the envelopes obtained using the *ab initio* program GASBOR[37] provides two important results.

(1) The $P(r)$ function of Mg^{2+}-Cdc31 (gray curve in Figure 6A) presents a shoulder around 40 Å, very similar to the shoulder observed in the $P(r)$ curve calculated from the crystal structure without peptide (red curve in Figure 6A). This shoulder is due to the interdistance between the N- and C-terminal domains and indicates that these domains are individualized, with an average interdistance of 40 Å. It is instructive to observe that this shoulder is almost completely absent for the apo-Cdc31 (black curve in Figure 6A). This reflects that the two domains are not individualized in the apo-protein whereas they are well separated in the Mg^{2+}-Cdc31. This is confirmed by the analysis of the envelopes obtained using GASBOR program. For each protein, 20 envelopes were determined and then superimposed with the chain of programs DAMAVER. The various envelopes are very similar since the NSD parameter (normalized spatial discrepancy) used to quantify their difference is about 1, which indicates a high reliability of the solutions. The most typical envelope is represented in Figures 6E and 6G for Mg^{2+}-Cdc31 and apo-Cdc31, respectively. Envelope E clearly shows a separation between both domains, which is absent in envelope G. It should be noted that this "groove" in Mg^{2+}-Cdc31 is probably underestimated insofar as the low affinity Mg^{2+} sites (see flow dialysis experiments) are not fully occupied at the experimental conditions. The filling of the "groove" between the two domains in the apo-form cannot originate from the position of the 13 residues N-terminal end (predicted disordered), as the Asn^{14} residue is located on the other side of the protein, opposed to the "groove", as shown in Figure 6C (arrow).

(2) The $P(r)$ function for R18-ScSfi1/Cdc31 complex is shown in Figure 6B, in comparison with that calculated from the crystal structure 2G5V (molecule B) with the peptide (the N-terminal M^1—L^{13} residues are missing, as mentioned previously). The calculated curve does not display any shoulder around 40 Å, as expected from our previous analysis, since the "groove" between the two domains is now occupied by the peptide. The remarkable fact is that the experimental curve very clearly shows an unexpected "bump" around 40 Å, indicating that the two domains are not in contact. To account for this effect, the N-terminal domain is slightly moved by using the program CORAL and by modeling together the N-terminal missing part. A variation by a few degrees of this domain leads to an excellent adjustment of the calculated curve to the experimental one (Figure 6H). Moreover, the structure thus obtained adapts perfectly to the most typical envelope obtained with programs GASBOR and DAMAVER (Figure 6F).

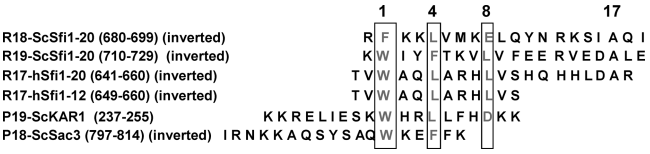

Figure 7. Amino acids sequences of the peptides used in this paper. Some peptides are in an inverted representation (C to N end) in order to indicate the 1—4—8 triad (in gray). The alignment of the peptides was made to take into account the superposition of anchoring 1—4—8 residues.

Interaction with Natural Peptides. ITC has been used to characterize the interaction between Cdc31 and their targets. We have used different peptides derived from the natural targets Kar1, Sfi1, and Sac3, such as P19-ScKar1, R18-ScSfi1, R19-ScSfi1, and P18-ScSac3 (Figure 7). The peptidic fragments of Kar1 and Sfi1 responsible for the interaction with centrins have been previously characterized (see Introduction) and shown to possess the conserved 1—4—8 triad. For the thermodynamic study of the interaction between ScSfi1 and Cdc31 we have selected two of the 21 identified repeats: R18 and R19. R18 contains a Phe in the first position (which is generally occupied by a Trp), and R19 has a Phe in the fourth position of the triad 1—4—8 (Figure 7). Phe is quite common (11/21) in the fourth position of the ScSfi1 repeats. The eighth amino acid in the triad is more variable (hydrophobic, polar, or charged residue). R18 has a Glu in the eighth position and is found in the R17-R18-ScSfi1/Cdc31 crystal structure (2GV5). The R18-ScSfi1 and R19-ScSfi1 synthetic peptides are 20 amino acid residues long and cover the N-terminal part of the repeats. The 17th residue position, numbered from first position of the triad (Figure 7), is also well conserved (generally a hydrophobic). This residue has contacts with the N-terminal domain of the Cdc31 in the crystal structure of the Cdc31/ScSfi1 complex.[17] When we wanted to study the Cdc31/ScSac3 interaction by ITC, we had no indication about which peptidic fragment of Sac3 was involved in the Cdc31 interaction. Therefore, we have used bioinformatics tools[38] to search for an amphipathic α-helix peptidic segment, with a 1—4—8 motif. We found a putative centrin binding motif in Sac3 protein: the segment 797—814. The corresponding peptide (K^{797}FFEKWQASYSQAKKNRI^{814}) was synthesized and tested by ITC. For all the interactions the Cdc31 was titrated by the peptides. Figure 8 shows the thermograms and the binding curves of the interactions tested (at 30 °C). All thermograms show a single site interaction. ITC data were fitted with a one site binding model. The thermodynamic parameters obtained are summarized in Table 3. For all tested peptides, strong interactions ($\sim 10^7$ M^{-1}) are observed in the presence of Ca^{2+}. Lower affinities are obtained for the apo- and Mg^{2+}-forms, i.e., 2 and 1 order of magnitude lower than for the Ca^{2+}-form. The Cdc31/target interactions are primarily mediated by the centrin C-terminal domain via the hydrophobic interactions with the C-terminal part of the Sfi1 repeat. The centrin N-terminal domain has only a reduced number of contacts with the Sfi1 repeats.[17] To characterize the role of the N-terminal Sfi1 segment for the Cdc31 interaction we tested, by ITC, the binding of Cdc31 to one human Sfi1 repeat (R17) containing or not the N-terminal fragment. For the two peptides tested, R17-hSfi1-20 (20 residues long) and R17-hSfi1-12 (12 residues long) (Figure 7), the thermodynamic parameters obtained are almost the same. The molecular recognition between Cdc31 and P18-ScSac3 has been followed by ITC and by changes in the emission of Trp

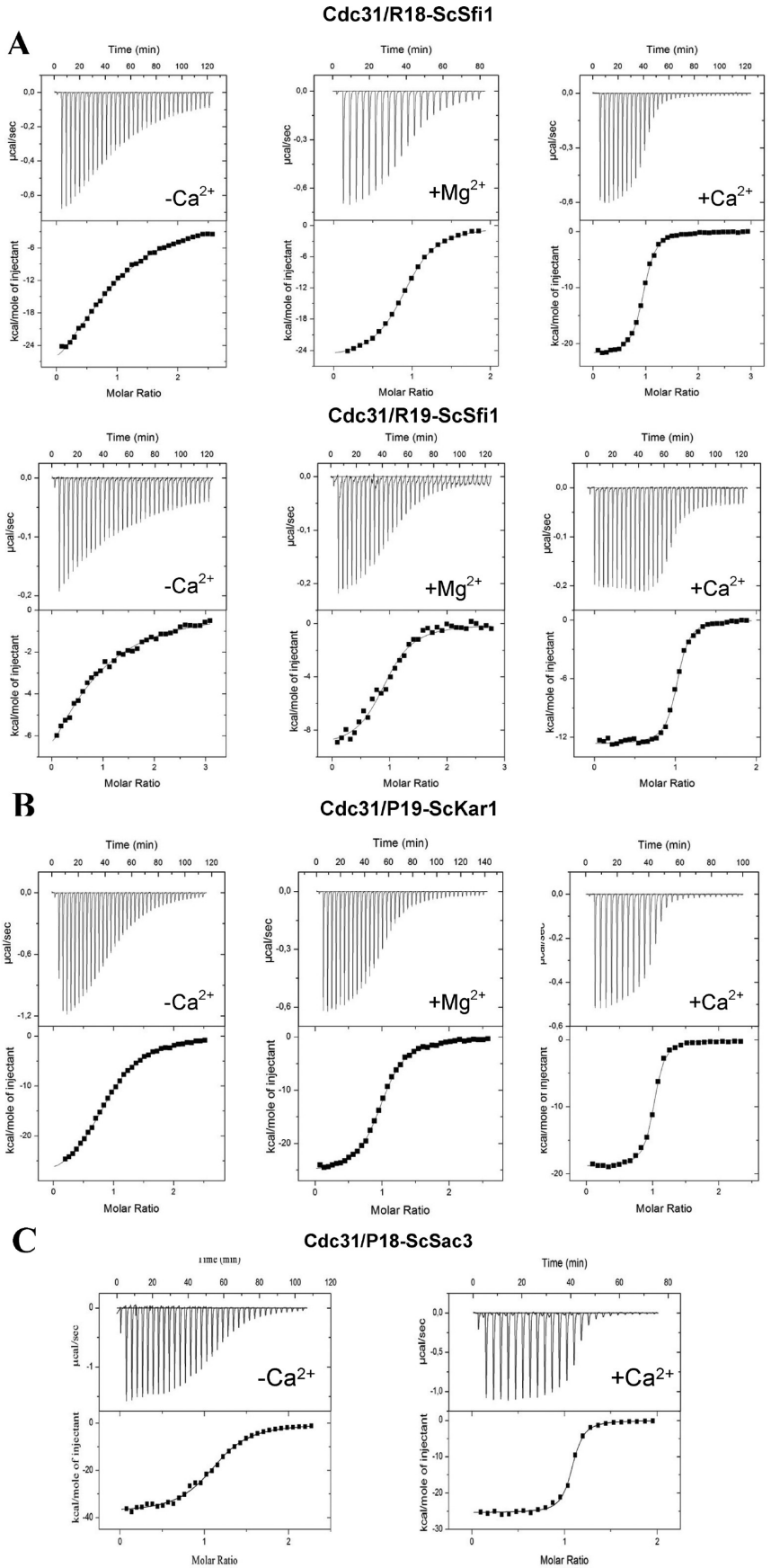

Figure 8. ITC thermograms and isotherms (at 30 °C) of binding of different natural target peptides to Cdc31. Titration of Cdc31 by R18-ScSfi1 and R19-ScSfi1 (A), P19-ScKar1 (B), and P18-ScSac3 (C) in the absence of Ca^{2+} (2 mM EDTA) and in the presence of Mg^{2+} (2 mM $MgCl_2$, 2 mM EGTA) or Ca^{2+} (2 mM $CaCl_2$).

dx.doi.org/10.1021/bi200518d |*Biochemistry* XXXX, XXX, 000–000

Table 3. Thermodynamic Data of the Interaction of Cdc31 with P19-ScKar1, R18-ScSfi1, R19-ScSfi1, P18-ScSac3, and R17-hSfi1 Peptides[a]

protein	Ca^{2+} (2 mM)	EDTA (2 mM)	Mg^{2+} (2 mM) 2 mM EGTA	peptide	K_a (±error) (M^{-1})	ΔG (kcal/mol)	ΔH (±error) (kcal/mol)	$T\Delta S$ (kcal/mol)	n
Cdc31	+			P19-ScKar1	2.3×10^7 (0.15)	−10.2	−18.8 (0.08)	−8.6	0.98
Cdc31			+	P19-ScKar1	3.6×10^6 (0.1)	−9.0	−25.5 (0.09)	−16.4	0.99
Cdc31		+		P19-ScKar1	4.4×10^5 (0.1)	−7.8	−29.7 (0.2)	−21.9	0.91
Cdc31	+			R18-ScSfi1	1.0×10^7 (0.03)	−9.7	−21.9 (0.07)	−12.2	0.93
Cdc31			+	R18-ScSfi1	2.9×10^6 (0.05)	−8.9	−25.7 (0.09)	−16.8	0.91
Cdc31		+		R18-ScSfi1	2.4×10^5 (0.13)	−7.5	−40.0 (1.2)	−32.5	0.94
Cdc31	+			R19-ScSfi1	3.5×10^7 (0.29)	−10.4	−12.7 (0.06)	−2.3	1.00
Cdc31			+	R19-ScSfi1	3.0×10^6 (0.04)	−9.0	−13.7 (0.41)	−4.7	0.68
Cdc31		+		R19-ScSfi1	1.9×10^5 (0.3)	−7.3	−14.0 (1.2)	−6.7	0.71
Cdc31	+			P18-ScSac3	2.2×10^7 (0.2)	−10.2	−25.4 (0.13)	−15.2	1.05
Cdc31		+		P18-ScSac3	1.5×10^6 (0.11)	−8.5	−37.9 (0.36)	−29.4	1.13
Cdc31	+			R17-hSfi1−20	3.9×10^6 (0.15)	−9.1	−19.2 (0.09)	−10.1	0.69
Cdc31			+	R17-hSfi1−20	1.4×10^5 (0.07)	−7.1	−20.7 (0.07)	−13.6	0.93
Cdc31		+		R17-hSfi1−20	∼mM				
Cdc31	+			R17-hSfi1−12	2.3×10^6 (0.08)	−8.8	−21.0 (0.13)	−12.2	0.69
HsCen2	+			P11-XPC	1.0×10^7 (0.03)	−9.7	−24.6 (0.06)	−14.9	0.95

[a] ITC experiments have been performed at 30 °C in 50 mM Mops buffer, pH 7.4, 100 mM NaCl.

fluorescence of P18-ScSac3 induced by Cdc31 binding (which lacks the Trp residue). The peptides were titrated by Cdc31, and the maximum of the observed fluorescence was shifted from 350 to 330 nm (data not shown). The intensity of Trp emission increased (at 330 nm) up to the saturation. These experiments clearly indicate that the P18-ScSac3 interact with Cdc31, the Trp being embedded in an apolar environment, such as the other Trp containing target peptides bound to centrins or to calmodulin. The fluorescence titration curve gives a dissociation constant of 0.1 μM for P18-ScSac3 (in the presence of calcium), very close to those obtained by ITC (Table 3).

DISCUSSION

As discussed before,[21] the CaM superfamily displays a bewildering diversity in the cation binding properties, including the affinity, kinetics, specificity, and cooperativity. Our data indicate that this is even true for the much more confined centrin subfamily. *Chlamydomonas reinhardtii* centrin kept three functional EF-hands, with one of the C-terminal sites showing a very low affinity.[23] HsCen2 evolved still further away from the prototypical CaM and binds only one Ca^{2+} per monomer with a moderate affinity (K_{dCa} = 30 μM) but strict Ca^{2+} specificity.[22] A particular truncated form of HsCen2, including the C-terminal half and helix D, can bind two Ca^{2+} ions in EF3 and EF4, as does also the entire protein in a complex with melittin.[22] HsCen3 displays one high affinity (K_{dCa} = 3 μM; K_{dMg} = 10 μM) Ca^{2+}/Mg^{2+} mixed site and two low affinity (K_{dCa} = 140 μM) Ca^{2+}-specific sites. The affinity of HsCen3 for Mg^{2+} is among the highest registered for the whole EF-hand Ca^{2+}-binding protein family.[21] In this study we show that Cdc31 displays several characteristics of HsCen3: one Ca^{2+}/Mg^{2+} mixed site (K_{dCa} = 0.3 μM; K_{dMg} = 44 μM) and two low affinity (K_{dCa} = 28 μM; K_{dCa} = 41 μM) Ca^{2+} sites. Mg^{2+} has an effect on the latter Ca^{2+} sites, but we are unable to distinguish between direct competition or an indirect (allosteric) effect, as the one that occurs in CaM, which is commonly considered to possess Ca^{2+}-specific sites. The affinity of Cdc31 for Ca^{2+} is distinctly higher and the affinity for Mg^{2+} much lower than in HsCen3. These quantitative differences may reflect differences in the Ca^{2+} homeostasis of yeast and man. In yeast Ca^{2+} influx is elicited by hyper- and hypotonic shock, cold and salt stress[39] and, as recently been reported,[40] oxidative stress. An increase in cytosolic Ca^{2+} has also been detected in budding yeast after mating pheromone treatment.[41] Despite earlier reports of weak Ca^{2+} signaling in yeast,[35] recently Ca^{2+}-dependent processes, such as the capacitative Ca^{2+} entry (CCE) at the plasma membrane and the unfolding response (UPR) in the endoplasmic reticulum, have been discovered in yeast.[42] Molecular components of a dynamic Ca^{2+} signaling have been evidenced, such as the plasma membrane Ca^{2+} channel Cch1p/Mid1p and the vacuolar Ca^{2+} channel Yvc1, the vacuolar Ca^{2+} pump Pmc1p, the golgi Ca^{2+} pump Pmr1p, and the vacuolar Ca^{2+}/3 H^+ exchanger Vcx1p/Hum1p.[40]

The three-dimensional structure of the complex of three Cdc31 molecules with a Sfi1 three-repeat showed Ca^{2+} bound at EF1, EF3, and EF4 of two of the Cdc31 units.[17] Geier et al.[25] showed that inactivation of EF1 or EF4 abolishes Ca^{2+}-dependent conformational changes and Cdc31's function in cell viability, whereas the inactivation of EF2 and EF3 did not influence these responses. Our study complements these former data and shows that Cdc31 has a high affinity Ca^{2+}/Mg^{2+} binding site and two low affinity Ca^{2+} sites. The Ca^{2+}/Mg^{2+} high affinity mixed site has an affinity, which is 10-fold higher and 4-fold lower for Ca^{2+} and Mg^{2+}, respectively, than in HsCen3.[a] In HsCen3 a remarkable feature is the critical role of the high affinity Ca^{2+}/Mg^{2+} mixed site in the conformational transition from a molten globule (MG) to a compact folded state.[21] *In vivo*, the permanent occupation of this site by a dication (Mg^{2+} in the relaxed and Ca^{2+} in the activated form) protects the protein from the MG state and from fast proteasomal degradation. The rationale for the evolutionary acquisition of such a Ca^{2+}/Mg^{2+} site in a sensor protein is double: either the site serves to anchor the sensor to a particular structure, such as TnC,[43] or it

dx.doi.org/10.1021/bi200518d |*Biochemistry* XXXX, XXX, 000–000

protects the protein from falling into the MG state and being degraded, such as HsCen3.[21]

Since the Ca^{2+}/Mg^{2+} high affinity mixed site in Cdc31 controls the Tyr fluorescence characteristics, it is likely that it is located in the N-terminal half of the protein. EF2 site does not appear to be active, since the EF2 motif displays an Arg instead of an oxygen-bearing group in position *Z* of the binding loop, a His instead of Gly in the central turn position, a Met instead of Ile/Leu in the short β-pleated sheet, and an Asp instead of Glu in the critical position $-Z$ (Figure 1B). EF1 motif could thus be assign as the Ca^{2+}/Mg^{2+} high affinity mixed site. Based on the fragment studies, the site EF1 in HsCen3, too, has been considered to be the Ca^{2+}/Mg^{2+} mixed site.[21] Therefore, we can speculate that the EF3 and EF4 are the low affinity Ca^{2+} sites.

Our CD studies yields information about the secondary structure and the thermal stability of Cdc31. While the apo-HsCen3 displays only ~27% residues in α-helix conformation,[21] the Cdc31 seems to have more structural organization in the apo-form (38.5% α-helices). Moreover, unlike the apo-HsCen3, the apo-Cdc31 shows a cooperative unfolding process. This indicates that the apo-Cdc31 adopts a less flexible conformation as compared to the molten globule apo-HsCen3 state.[21] The addition of Ca^{2+} and Mg^{2+} induces a secondary structural organization and a thermal stabilization of Cdc31. Most sensor CaBPs, such as CaM, are well-folded in the apo state, with no hydrophobic residues exposed to the solvent. Upon binding of Ca^{2+}, most CaBPs of the sensor type—but not the Ca^{2+} buffering proteins such as parvalbumins—exhibit a hydrophobic exposure on the surface, allowing interaction with the target proteins. Unlike the CaM, the apo-Cdc31 exposes hydrophobic surface area, as indicated by TNS fluorescence results. A significant fluorescence of TNS is observed for the Mg^{2+}- and Ca^{2+}-Cdc31 but also for the apo-Cdc31. As indicated by our ITC experiments, Mg^{2+} and Ca^{2+} binding also affect (increase) the affinity of protein to peptides (Table 3). Nevertheless, *in vitro* and within the concentration range used in our experiments, Mg^{2+} and Ca^{2+} binding does not seem to be critical for the interactions with target proteins since apoprotein could also interacts with the peptides which we tested. However, the interactions of target proteins with Cdc31 in the cell conditions, at rest ion concentrations, may not be considered until the *in vivo* protein intracellular concentrations are not carefully estimated.

Small-angle X-ray scattering (SAXS) experiments complement our knowledge on centrin structures and provide new information about the Cdc31 conformations in solution on changes that take place upon ligands (ions or/and target) binding. The full-length apo-centrin structures have not been determined until now by X-ray crystallography or NMR, probably due to their high flexibility. Despite this flexibility, we show here that the N- and C-terminal domains of apo-Cdc31 are in close vicinity, likely fused together. The addition of Mg^{2+} allows their individualization. This more open conformation could thus be helpful for the interaction of protein with their targets. Our SAXS characterization of the R18-ScSfi1/Cdc31 complex demonstrate that Cdc31 could adopt a slight more open conformation in solution (the N-terminal domain could move) as compared to the crystal structure. In the same direction our ITC data provide evidence that the contacts between the N-terminal Cdc31 domain and the N-terminal Sfi1 repeat are not important for the complex formation. The interaction between the N-terminal Cdc31 domain and the N-terminal Sfi1 peptide could be thus absent in solution. These contacts, which are observed in the crystal structure, are a consequence of the central linker bent of Cdc31 (due to the presence of a proline residue, Pro^{94}, in the central linker) and are probably encouraged by the crystal lattice. An equivalent proline (Pro^{99}) is also present in the central linker region of the HsCen3, suggesting that similar structural characteristics might exist in the homologous human centrin HsCen3. Similarly, fewer contacts have been observed between Sac3 and N-terminal Cdc31 domain[26] as compared to the crystal structure of Cdc31/ScSfi1.[17]

The yeast Cdc31 centrin is involved in different cellular functions, interacting with different targets, such as Sfi1 or Kar1 in the SPB or the Sac3, a nuclear pore-associated protein. The understanding of the regulation of these different functions by Cdc31 requires a detailed thermodynamic characterization of these interactions. ITC thermodynamics gave information on the physical forces involved as well as on the role of triad residues (1−4−8) in the interaction between Cdc31 and different natural target peptides. All interactions are enthalpically driven, with an important exothermic heat exchange (favorable enthalpy term), indicating that polar processes (like favorable hydrogen bond contacts, van der Waals, etc.) must be important, in addition to the hydrophobic contacts previously shown to be important for centrin complex formation.[17,18,27] Hydrogen bonds have been observed between centrins and targets in the X-ray complex structures, generally between the acidic centrin residues (Asp) and the charged basic residues of the peptidic targets. The entropic term is negative (unfavorable), associated with the conformational transitions observed in the peptides and the protein upon complex formation, from a flexible to more structured forms.[27] As mentioned, the Mg^{2+}- and apo-form of Cdc31 have 1 and 2 order of magnitude lower affinities for the target peptides than the Ca^{2+}-form. For Kar1/Cdc31 interaction, the affinity obtained by ITC in buffers containing 2 mM Ca^{2+} was similar to those obtained by Geier et al.[25] at 1.35 μM of Ca^{2+}. ITC affinity is 50 times lower in the absence of calcium. Geier et al.[25] have also observed that the affinity of Cdc31 for Kar1 decreases (20-fold) at 0.038 μM of Ca^{2+}. Cdc31 could bind targets even in the absence of Ca^{2+} and therefore shows a modest Ca^{2+} sensitivity, a general characteristic of all centrins.[24,27]

Many sensor CaBPs are poorly sensitive to Mg^{2+}. In CaM, the presence of Mg^{2+} increases the thermodynamic stability of the protein, without a significant structural effect (the exposure of a hydrophobic surface) required for the interaction with targets.[44,45] While Mg^{2+}-CaM binds peptides with slightly lower affinity than apo-CaM,[44] the role of Mg^{2+} in Cdc31 seems to be different. Mg^{2+} has not only an effect on the Cdc31 conformation but also on the stability and the interaction of the protein with targets, like Kar1 and Sfi1. HsCen3 has also the ability to bind Mg^{2+} ions. The native PAGE experiments showed qualitatively a binding of melittin peptide to HsCen3 in the presence of 1 mM Mg^{2+} and EGTA.[21] However, the binding affinity of Mg^{2+}-HsCen3 for the target peptides has not been characterized. The affinity of Cdc31 for SPB targets is 10 times higher in the presence of Mg^{2+} than in the apo-form.

Calorimetric titrations of Cdc31 by R18-ScSfi1 and R19-ScSfi1 peptides provided similar thermodynamic parameters. This indicates that each repeat is capable to bind one molecule of Cdc31, as was already shown by pull-down experiments.[16] The replacement of Trp_1 by a Phe, and of Leu_8 by a Glu, in the R18-ScSfi1 has no significant effect on the affinity of binding. The substitution of Trp_1 by another hydrophobic residue (Leu) in the R9-hSfi1 repeat showed no effect on HsCen2/R9-hSfi1

interaction.[46] The drastic change of a hydrophobic residue with a charged one, in the eighth position of the R18-ScSfi1 and the P19-ScKar1 peptides (Leu_8 replaced by Glu and Asp, respectively) also does not influence the affinity constants for Cdc31. The P17-XPC ($L^{855}A$) variant (where Leu_8 was replaced by an Ala) showed also an unchanged binding free energy.[27] The eighth residue of the triad in the centrin binding motif seems to be less important for centrin binding. Recently, the available crystal structure of Cdc31 bound to Sac3[26] showed a reverse binding motif in Sac3 (like in ScSfi1), with a basic residue (Arg) in the eighth position of the triad. The P18-ScSac3 peptide (tested here by calorimetry) does not have the eighth residue of the triad and shows a high affinity constant for Cdc31 in the absence or in the presence ($K_a = 2.2 \times 10^7\ M^{-1}$) of Ca^{2+}. This was not the case for the minimal sequences (containing only 1−4 residues of the triad) of centrin-binding peptides tested, as the P5-XPC (847−851) and the R17-hSfi1-6 (655−660). These peptides have weak affinity constants for centrins, in the presence of Ca^{2+} ($K_a = 2.5 \times 10^5\ M^{-1}$ and $K_a < 10^4\ M^{-1}$, respectively). Although the 805−815 fragment of the ScSac3 peptide was shown not to be necessary *in vitro* for Cdc31 binding,[25] it enabled the P18-ScSac3/Cdc31 interaction to be significant. The entropic term for P5-XPC(847−851)/HsCen2 interaction is positive (favorable),[27] whereas for P18-ScSac3/Cdc31 interaction is negative (unfavorable). A longer sequence could efficiently stabilize the bound peptide (in a α-helix) and the protein in the complex. To test this hypothesis, we have synthesized and characterized by ITC the interaction between HsCen2 and P11-XPC peptide (R^{843}ALGNWKLLAK^{853}), containing the 1−4 hydrophobic residues of the triad. This peptide, containing 11 residues, is longer (in the N-terminal end) than P5-XPC. The affinity (in the presence of calcium) is $1.03 \times 10^7\ M^{-1}$ (Table 3), which is about 2 orders of magnitude higher than the affinity for P5-XPC. The bulky hydrophobic residues, 1 and 4, of the triad are thus critical for centrin binding and serve as key anchor points. The α-helix organization of the centrin binding motif is necessary to correctly point the hydrophobic 1−4 side-chains of the target surface for the interaction with centrin.

CONCLUSIONS

In general, few Ca^{2+} sensors have been reported in yeast (calcineurin seems to be a major one). CaM has been considered as vital for SPB duplication and for mRNA export but is functional without the need for Ca^{2+} binding.[47] What about the yeast centrin function *in vivo*? We showed that Cdc31 bind Ca^{2+}, but also Mg^{2+} ions, and this has a structural effect on Cdc31 and induced a structural stabilization of the protein. We provided evidence that yeast centrin can bind targets, *in vitro*, even in the absence of ions binding. Interestingly, the Cdc31 is sensitive to Mg^{2+}, an ion which is present in millimolar concentrations inside the cells. Mg^{2+} ions affect the Cdc31 conformation, and this seems to be helpful for target binding. Indeed, a higher affinity of binding of target peptides to Cdc31 is observed in the presence of concentrations of Mg^{2+} which are similar to the intracellular concentrations.

We note that in the presence of high Mg^{2+} concentration the self-assembly (polymers which are generally formed at high Ca^{2+} concentration) of Cdc31 are not observed. The post-translational modifications in Cdc31, such as ubiquitination, were shown to influence the Cdc31 function and prevent the oligomerization of centrins.[8] Mg^{2+} could be also an important functional factor to stimulate the interactions of Cdc31 in resting cells or to prevent the self-assembly (aggregation) of Cdc31 *in vivo*.

AUTHOR INFORMATION

Corresponding Author

*Phone: +33(0)169087135; Fax: +33(0)169084712; e-mail: simona.miron@cea.fr.

Present Addresses

⊥LBSR, Bât. 144, iBiTec-S, SB2SM, URA2096, CEA Saclay, 91190 Gif-s-Yvette, France.

#Faculty of Physics, University of Bucharest, Romania.

Funding Sources

This work was supported by the Institut National de la Santé et de la Recherche Médicale, the Centre National de la Recherche Scientifique and Institut Curie. C.C was a recipient of a FEBS fellowship.

Notes

&Deceased.

ACKNOWLEDGMENT

We dedicate this article in memoriam to Dr. Gil Craescu, *a passionate and distinguished scientist*, our colleague *who passed away prematurely*. We thank Isabelle Durussel and Jos Cox (Department of Biochemistry, University of Geneva) for assistance with the flow-dialysis and fluorescence experiments and in particular Jos Cox for enlightening scientific discussions and his significant help in editing the manuscript. We acknowledge SOLEIL for provision of synchrotron radiation facilities and Pierre Roblin for assistance during experiments on SWING beamline. We thank Cecile Merigoux for the SAXS technical assistance.

ABBREVIATIONS

HsCen1 to HsCen3, human centrin isoforms 1 to 3; Cdc31, *Saccharomyces cerevisiae* centrin; CrCen, *Chlamydomonas reinhardtii* centrin; SdCen, *Scherffelia dubia* centrin; CaM, calmodulin; Sfi1, suppressor of fermentation induced loss of stress resistance protein1; ScSfi1, *Saccharomyces cerevisiae* Sfi1; hSfi1, human Sfi1; CaBPs, calcium binding proteins; P19-ScKar1p, peptide K^{237}−K^{255} of yeast Kar1p; P17-XPC, peptide N^{847}-R^{863} of human XPC protein; P18-ScSac3, peptide K^{797}−I^{814} of yeast Sac3; R18-ScSfi1 and R19-ScSfi1, peptides I^{680}−R^{699} and E^{710}−K^{729} of yeast Sfi1, respectively; R17-hSfi1−20, peptide R^{641}-T^{660} of human Sfi1; P11-XPC, peptide R^{843}-K^{853} of human XPC; MG, molten globule; SPB, spindle pole body; TNS: 2-*p*-toluidinylnaphtalene-6-sulfonate; TnC, troponin C; ITC, isothermal titration calorimetry; CD, circular dichroism; SAXS, small-angle X-ray scattering; MTOC, microtubule organizing centers; NER, nucleotide excision repair.

ADDITIONAL NOTE

[a] Note that in the case of HsCen3 the high affinity site could not be titrated by Ca^{2+} at Mg^{2+} concentrations above 0.2 mM.[21] This is not the case for Cdc31, which has a much higher affinity for Ca^{2+}, and a much lower one for Mg^{2+}.

REFERENCES

(1) Schiebel, E., and Bornens, M. (1995) In search of a function for centrins. *Trends Cell Biol. 5*, 197–201.

(2) Salisbury, J. L., Suino, K. M., Busby, R., and Springett, M. (2002) Centrin-2 is required for centriole duplication in mammalian cells. *Curr. Biol. 12*, 1287–1292.

(3) Sanders, M. A., and Salisbury, J. L. (1994) Centrin plays an essential role in microtubule severing during flagellar excision in *Chlamydomonas reinhardtii*. *J. Cell Biol. 124*, 795–805.

(4) Araki, M., Masutani, C., Takemura, M., Uchida, A., Sugasawa, K., Kondoh, J., Ohkuma, Y., and Hanaoka, F. (2001) Centrosome protein centrin 2/caltractin 1 is part of the *Xeroderma pigmentosum* group C complex that initiates global genome nucleotide excision repair. *J. Biol. Chem. 276*, 18665–18672.

(5) Miron, S., Duchambon, P., Blouquit, Y., Durand, D., and Craescu, C. T. (2008) The carboxy-terminal domain of *Xeroderma pigmentosum* complementation group C protein, involved in TFIIH and centrin binding, is highly disordered. *Biochemistry 47*, 1403–1413.

(6) Resendes, K. K., Rasala, B. A., and Forbes, D. J. (2008) Centrin 2 localizes to the vertebrate nuclear pore and plays a role in mRNA and protein export. *Mol. Cell. Biol. 28*, 1755–1769.

(7) Fischer, T., Rodriguez-Navarro, S., Pereira, G., Racz, A., Schiebel, E., and Hurt, E. (2004) Yeast centrin Cdc31 is linked to the nuclear mRNA export machinery. *Nat. Cell Biol. 6*, 840–848.

(8) Chen, L., and Madura, K. (2008) Centrin/Cdc31 is a novel regulator of protein degradation. *Mol. Cell. Biol. 28*, 1829–1840.

(9) Spang, A., Courtney, I., Fackler, U., Matzner, M., and Schiebel, E. (1993) The calcium-binding protein cell division cycle 31 of *Saccharomyces cerevisiae* is a component of the half bridge of the spindle pole body. *J. Cell Biol. 123*, 405–416.

(10) Paoletti, A., Bordes, N., Haddad, R., Schwartz, C. L., Chang, F., and Bornens, M. (2003) Fission yeast cdc31p is a component of the half-bridge and controls SPB duplication. *Mol. Biol. Cell 14*, 2793–2808.

(11) Adams, I. R., and Kilmartin, J. V. (2000) Spindle pole body duplication: a model for centrosome duplication? *Trends Cell Biol. 10*, 329–335.

(12) Byers, B. (1981) Multiple roles of the spindle pole bodies in the life cycle of *Saccharomyces cerevisiae*. *Molecular Genetics in Yeast*, Alfred Benzon Symposium 16 (von Wettstein, D., Friis, J., Kielland-Brand, M., and Stenderup, A., Eds.) pp 119−131, Munksgaard, Copenhagen, Denmark.

(13) Biggins, S., and Rose, M. D. (1994) Direct Interaction between Yeast Spindle Pole Body Components: Karlp Is Required for Cdc31p Localization to the Spindle Pole Body. *J. Cell Biol. 4*, 843–852.

(14) Spang, A., Courtney, I., Grein, K., Matzner, M., and Schiebel, E. (1995) The Cdc31p- binding protein Kar1p is a component of the half bridge of the yeast spindle pole body. *J. Cell Biol. 128*, 863–877.

(15) Jaspersen, S. L., Giddings, J. T. H., and Winey, M. (2002) Mps3p is a novel component of the yeast spindle pole body that interacts with the yeast centrin homologue Cdc31p. *J. Cell Biol. 159*, 945–956.

(16) Kilmartin, J. V. (2003) Sfi1p has conserved centrin-binding sites and an essential function in budding yeast spindle body duplication. *J. Cell Biol. 162*, 1211–1221.

(17) Li, S., Sandercock, A. M., Conduit, P., Robinson, C. V., Williams, R. L., and Kilmartin, J. V. (2006) Structural role of Sfi1p-centrin filaments in budding yeast spindle pole body duplication. *J. Cell Biol. 173*, 867–877.

(18) Martinez-Sanz, J., Yang, A., Blouquit, Y., Duchambon, P., Assairi, L., and Craescu, C. T. (2006) Binding of human centrin 2 to the centrosomal protein hSfi1. *FEBS J. 273*, 4504–4515.

(19) Popescu, A., Miron, S., Blouquit, Y., Duchambon, P., and Craescu, C. T. (2003) *Xeroderma pigmentosum* group C protein possesses a high affinity binding site for human centrin 2 and calmodulin. *J. Biol. Chem. 278*, 40252–40261.

(20) Nishi, R., Okuda, Y., Wanatabe, E., Mori, T., Iwai, S., Masutani, C., Sugasawa, K., and Hanoka, F. (2005) Centrin 2 stimulates nucleotide excission repair by interacting with *Xeroderma pigmentosum* group C protein. *Mol. Cell. Biol. 25*, 5664–5674.

(21) Cox, J. A., Tirone, F., Durussel, I., Firanescu, C., Blouquit, Y., Duchambon, P., and Craescu, C. T. (2005) Calcium and magnesium binding to human centrin 3 and interaction with target peptides. *Biochemistry 44*, 840–850.

(22) Durussel, I., Blouquit, Y., Middendorp, S., Craescu, C. T., and Cox, J. A. (2000) Cation- and peptide-binding properties of human centrin 2. *FEBS Lett. 472*, 208–212.

(23) Veeraraghavan, S., Fagan, P. A., Hu, H., Lee, V., Harper, J. F., Bessie, H., and Chazin, W. J. (2002) Structural independence of the two EF-hand domains of caltractin. *J. Biol. Chem. 277*, 28564–28571.

(24) Radu, L., Durussel, I., Assairi, L., Blouquit, Y., Miron, S., Cox, J. A., and Craescu, C. T. (2010) *Scherffelia dubia* centrin exhibits a specific mechanism for Ca^{2+}-controlled target binding. *Biochemistry 49*, 4383–4394.

(25) Geier, B. M., Wiech, H., and Schiebel, E. (1996) Binding of centrins and yeast calmodulin to synthetic peptides corresponding to binding sites in the spindle pole body components Kar1p and Spc110p. *J. Biol. Chem. 271*, 28366–28374.

(26) Jani, D., Lutz, S., Marshall, N. J., Fischer, T., Köhler, A., Ellisdon, A. M., Hurt, E., and Stewart, M. (2009) Sus1, Cdc31, and the Sac3 CID region form a conserved interaction platform that promotes nuclear pore association and mRNA export. *Mol. Cell 33*, 727–737.

(27) Charbonnier, J. B., Renaud, E., Miron, S., Le Du, M. H., Blouquit, Y., Duchambon, P., Christova, P., Shosheva, A., Rose, T., Angulo, J. F., and Craescu, C. T. (2007) Structural, thermodynamic, and cellular characterization of human centrin 2 interaction with *Xeroderma pigmentosum group C* protein. *J. Mol. Biol. 373*, 1032–1046.

(28) Colowick, S. P., and Womack, F. C. (1969) Binding of diffusible molecules by macromolecules: rapid measurement by rate of dialysis. *J. Biol. Chem. 244*, 774–747.

(29) Cox, J. A. (1996) in *Guidbook to the Calcium-Binding Proteins* (Celio, M. R., Pauls, T., and Schwaller, B., Eds.) pp 1−12, Oxford University Press, Oxford.

(30) Sreerama, N., and Woody, R. W. (2000) Estimation of protein secondary structure from circular dichroism spectra: comparison of CONTIN, SELCON and CDSSTR methods with an expanded reference set. *Anal. Biochem. 287*, 252–260.

(31) David, G., and Pérez, J. (2009) Combined sampler robot and high-performance liquid chromatography: a fully automated system for biological small-angle X-ray scattering experiments at the Synchrotron SOLEIL SWING beamline. *J. Appl. Crystallogr. 42*, 892–900.

(32) Mertens, H. D., and Svergun, D. I. (2010) Structural characterization of proteins and complexes using small-angle X-ray solution scattering. *J. Struct. Biol. 172*, 128–141.

(33) Milos, M., Schaer, J. J., Comte, M., and Cox, J. A. (1986) Calcium-proton and calcium-magnesium antagonisms in calmodulin: microcalorimetric and potentiometric analyses. *Biochemistry 25*, 6279–6287.

(34) Tanaka, T., and Hidaka, H. (1980) Hydrophobic regions function in calmodulin-enzyme(s) interactions. *J. Biol. Chem. 255*, 11078–11080.

(35) Davis, T. N. (1995) Calcium in *Saccharomyces cervisiae*. *Adv. Second Messenger Phospoprotein Res. 30*, 339–358.

(36) Svergun, D. I. (1992) Determination of the regularization parameter in indirect-transform methods using perceptual criteria. *J. Appl. Crystallogr. 25*, 495–503.

(37) Svergun, D. I., Petoukhov, M. V., and Koch, M. H. (2001) Determination of domain structure of proteins from X-ray solution scattering. *Biophys. J. 80*, 2946–2953.

(38) Yap, K. L., Kim, J., Truong, K., Sherman, M., Yuan, T., and Ikura, M. (2000) Calmodulin Target Database. *J. Struct. Funct. Genomics 1*, 8–14.

(39) Matsumoto, T. K., Ellsmore, A. J., Cessna, S. G., Low, P. S., Pardo, J. M., Bressnan, R. A., and Hasegawa, P. M. (2002) An osmotically induced cytosolic Ca^{2+} transient activates calcineurin signaling to mediate ion homeostasis and salt tolerance of *Saccharomyces cerevisiae*. *J. Biol. Chem. 277*, 33075–33080.

(40) Popa, C. V., Dumitru, I., Ruta, L. L., Danet, A. F., and Farcasanu, I. C. (2010) Exogenous oxidative stress induces Ca2+ release in the yeast Saccharomyces cerevisiae. *FEBS J. 277*, 4027–4038.

(41) Iida, H., Nakamura, H., Ono, T., Okumura, M. S., and Anraku, Y. (1994) MID1, a novel *Saccharomyces cerevisiae* gene encoding a plasma membrane protein, is required for Ca^{2+}- influx and mating. *Mol. Cell. Biol. 14*, 8259–8271.

(42) Bonilla, M., Nastase, K., and Cunningham, K. W. (2002) Essential role of calcineurin in response to endoplasmic reticulum stress. *EMBO J. 21*, 2343–2353.

(43) Cox, J. A., Comte, M., and Stein, E. A. (1981) Calmodulin-free skeletal muscle troponin C prepared in the absence of urea. *Biochem. J. 195*, 205–311.

(44) Haiech, J., Klee, C. B., and Demaille, J. G. (1981) Effects of cations on affinity of calmodulin for calcium: ordered binding of calcium ions allows the specific activation of calmodulin-stimulated enzymes. *Biochemistry 20*, 3890–3897.

(45) Martin, S. R., Masino, L., and Bayley, P. M. (2000) Enhancement by Mg^{2+} of domain specificity in Ca^{2+}-dependent interactions of calmodulin with target sequences. *Protein Sci. 9*, 2477–2488.

(46) Martinez-Sanz, J., Kateb, F., Assairi, L., Blouquit, Y., Bodenhausen, G., Abergel, D., Mouawad, L., and Craescu, C. T. (2010) Structure, Dynamics and Thermodynamics of the human Centrin 2/hSfi1 complex. *J. Mol. Biol. 395*, 191–204.

(47) Geiser, J. R., van Tuinen, D., Brockerhoff, S. E., Neff, M. M., and Davis, T. N. (1991) Can calmodulin function without binding calcium?. *Cell 65*, 1–20.

(48) Corpet, F. (1988) Multiple sequence alignment with hierarchical clustering. *Nucleic Acids Res. 16*, 10881–10890.

(49) Gouet, P., Courcelle, E., Stuart, D. I., and Metoz, F. (1999) ESPript: multiple sequence alignments in PostScript. *Bioinformatics 15*, 305–308.